Delithiation-induced Oxygen Vacancy Formation Causes Microcracking of $LiCoO_2$ Cathodes

Najma Yaqoob, Robert Mücke, Olivier Guillon, and Payam Kaghazchi*

*Corresponding author

Forschungszentrum Jülich GmbH, Institute of Energy and Climate Research, Materials Synthesis and Processing (IEK-1), Jülich, Germany

Emails: n.yaqoob@fz-juelich.de, r.muecke@fz-juelich.de, o.guillon@fz-juelich.de, p.kaghazchi@fz-juelich.de

Abstract

Cracking of cathode materials during cycling is a main cause of capacity fading in Li-ion batteries. In this work, by performing atomistic and microscale simulations, we study the possible reason behind the cracking of Li_xCoO_2 (LxCO) microstructures. It is shown that tensile uniaxial lattice strains larger than 2% along the *c*-direction (ε_c) can cause displacement of Li ions and a yield drop in the stress-strain $\sigma_c(\varepsilon_c)$ plot in LxCO. By modelling a typical microstructure consisting of packed microparticles and performing continuum mechanical analysis on the mesoscale we found that the electrochemically-induced (L1.00CO $\rightarrow$ L0.50CO) mechanical ε_c in the microstructure is, however, only $-2.5\% \leq \varepsilon_c \leq +0.5\%$. Moreover, we found that even a sharp space charge region cannot cause any significant local tensile strain. However, a small amount of oxygen vacancy (V_O^x) introduces a large local strain of $\varepsilon_c = 3\%$ leading to the displacements of Li ions. Furthermore, we found that the formation of V_O^x becomes more favourable with delithiation (L1.00CO $\rightarrow$ L0.50CO). The results of this work, thus, indicate that the delithiation-induced formation of V_O^x, which is a well-known phenomenon observed experimentally in operating cathode materials, is a main reason of microcracking of Li-based layered cathodes.

Introduction

$LiCoO_2$ (LCO) as a cathode material for Li-ion batteries was proposed in 1980 by Mizushima and Goodenough.[1] It is still one of the most popular and widely used compound for energy storages in electronic devices. LCO has a layered crystal structure (with a rhombohedral space group: R-3m) in which Li-ions deintercalate/intercalate from/into Li sites between slabs of CoO_6 octahedra during charge/discharge.[2] In principle, it can provide a long cycle life and high electronic conductivity. A main drawback of this system is its low practical energy density due to a structural instability occurring when more than 0.5 Li is extracted. In practice, only about a 0.5 Li content can be removed from LCO which gives a specific capacity of about 140 mAh/g with an upper cutoff voltage of about 4.2 V.[3] Wang *et al*.[4] performed a Transmission Electron Microscopy (TEM) study on LCO and reported that after 50 cycles, 20% of the particles were indeed fractured between 2.5 V and 4.35 V at a 0.2 C rate. Yoon *et al*.[5] studied this system by using the soft X-ray absorption spectroscopy and showed that the capacity experiences fading by 2.2% and 6.5% for a delithiation of 0.5 Li per CoO_2 after 10 and 50 charge-discharge cycles, respectively. It is believed that the changes in lattice parameters cause an irreversible damage of LCO structure, in particular the collapse of structure along the *c* direction[6], leading to cracking and failure, and thereby the capacity fading. Zhou *et al*.[6] performed an *in situ* XRD experiment to determine the variation of lattice parameters of LCO during delithiation i.e. Li_xCoO_2 (LxCO*,* x=1.0 and 0.5). They observed a contraction of 0.2% (a=2.82 Å → 2.81 Å) along the *a*-axis, while an expansion of 1.99% (c=14.09 Å → 14.37 Å) along the *c*-axis when x=1.0→0.5. A similar experiment by Amatucci *et al*.[7] indicates that the lattice parameter *a* contracts by ∼0.18% when x=1.0 → 0.6 followed by a subsequent increase of 0.24% when x=0.4 → 0.0. However, the *c* parameter experiences an expansion of 1.8% for x=1.0 → 0.5 followed by a contraction of −1.8% for x=0.5 → 0.2[7]. *Ex situ* X-Ray Diffraction (XRD) studies by Chen *et al*.,[3] Amatucci *et al*.,[7] and Ohzuku *et al*.[8] on L_xCO showed that when x=1.0 → 0.25, i.e. V= 4.2 → 4.8 V, a phase transition from the initial as synthesized O3 phase (oxygen stacking of ⋯ABCABC⋯) to a stage-two phase (H1-3) occurs. Chen *et al*.[3] measured the composition of H1-3 phase to be $Li_{0.12}CoO_2$ (a= 2.82 Å and c= 13.54 Å). Finally, Amatucci *et al*.[7] observed a further phase transition from O3-LxCO to O1-CoO_2 (oxygen stacking of ⋯ABAB⋯) for U= 5.2 V. Qu *et al*.[9] and Cheng *et al*.[10] performed nanomechanical measurement of plastic, fracture, and elastic properties of LCO using a nanoindentation test. They measured Young's modulus to be in the range of 151–236 GPa[9,10]. Feng *et al*.[11]

Tab. 1 Calculated mechanical properties of LxCO with different defect types and Li concentrations: bulk modulus (B), shear modulus (G), and Young's modulus (Y) in GPa as well as Poisson's ratio (ν). The subscripts V and R represents the results using Voigt-Reuss-Hill homogenization scheme[22]. Experimental values are listed for comparison.

	***X*=1**	***X*=1** $\mathbf{V_{Li}^{\times}}$	**X=1** $\mathbf{V_{Co}^{\times}}$	***X*=1** $\mathbf{V_{O}^{\times}}$	***X*=0.5**	***X*=0.12**	***X*=0**	**Exp**
$\mathbf{B_V}$	161.32	155.59	152.49	153.31	144.62	142.21	129.39	
$\mathbf{B_R}$	157.54	150.93	142.68	139.66	137.78	119.88	119.70	
B	159.43	153.26	147.58	146.49	141.20	131.04	124.55	149±[31]
$\mathbf{G_V}$	101.90	102.26	96.34	99.06	85.80	88.31	74.38	
$\mathbf{G_R}$	97.41	91.40	84.88	84.02	78.79	72.09	71.56	
G	99.66	96.83	90.61	91.54	82.29	80.20	72.97	80±1[30]
Y	247.43	239.96	225.65	227.27	206.72	199.84	183.15	151-236[9]
$\boldsymbol{\nu}$	0.24	0.24	0.24	0.24	0.25	0.25	0.25	0.23[29], 0.24[30]

studied the effect of electrochemical cycling on the strength of LCO using a TEM–based nanopillar compression experiment. They estimated that this system can withstand an ultimate strength in the range of 5.62 ± 0.22 GPa, 3.91 ± 1.22 GPa, and 2.27 ± 1.07 GPa for pristine and after 1 and 11 cycles, respectively.

First principles density functional theory (DFT) has also been applied to compute phase transition, lattice parameters, and the mechanical properties of L_xCO cathode materials.[11-14] For example, using DFT-LDA, Ceder *et al*.[12] calculated formation energies to simulate the staging phase transitions (O3-phase→H1-3-phase→ O1-phase) in L_xCO that were proposed by experimental works of Ohzuku *et al*.[8] and Amatucci *et al*.[7] Arup *et al*.[15] calculated (with DFT-PBE) changes in the lattice parameters of L*x*CO to be *a*=2.85 Å→2.82 Å→2.83 Å and *c*=14.05 Å→14.42 Å→14.21 Å for x=1.0→0.5→0.0. Qi *et al*.[13] using HSE06, while Feng *et al.*[11] and Wu *et al.*[14] using DFT-PBE computed the mechanical properties of L_xCO during Li insertion/deinsertion. They found that Young's modulus decreases dramatically from 264 GPa to 59.8 GPa during the deintercalation of *x*=1.0 → 0.0[13]. The bulk modulus *B* and shear modulus *G* decrease significantly from 166.74 GPa to 68.69 GPa and from 111.38 GPa to 41.71 GPa respectively.[14] Feng *et al*.[11] calculated (with DFT-PBE) the ultimate tensile strength for L_xCO by introducing Li vacancies heterogeneously on a single plane in the crystal. They showed that the strength, defined by the maximum stress that can be generated by applying strain, decreases from 33.7 GPa to 12.7 GPa when *x*=1.0 → 0.5. They reported that the critical strain, up to which the material can accommodate the arising stress before it experiences restructuring and stress drops with applying larger strain fields, is 33% and 8% for *x*=1.0 and 0.5, respectively. However, according to the DFT-PBE study by Wu *et al*.[14] the strength decreases from 40 GPa to 32 GPa (and critical strains from 32% to 30%) with the delithiation of *x*=1.0 → 0.5. The previously calculated values of strengths with DFT calculation are significantly larger than the experimental ones. Moreover, the proposed critical strain values above which the layered cathode materials experience cracking are considerably higher than the delithiation-induced contraction or expansion of lattice parameters. Direction and maximum possible magnitude of electrochemically-driven strain/stress generation in a microstructure of LCO have not been modelled so far. This information is required to find out if microstructuring is the reason of cracking. Moreover, the impact of point defects

has not been investigated. In this work, we address these issues by combining extensive DFT calculations as well as microstructure modelling and electrochemo-mechanical analysis on the grain level.

Method

Spin-polarized DFT calculations were performed using the projector augmented wave (PAW)[16] potential method implemented in the Vienna *Ab Initio* Simulation Package (VASP) code[17]. The Perdew–Burke–Ernzerhof (PBE)[18] form of generalized gradient approximation (GGA) was used as the exchange-correlation functional. We also checked the influence of adding a Hubbard *U* (Dudarev *et al*. approach[19]: *U-J*=5.9 eV for Co[20]) and dispersion D3[21] correction on the mechanical properties. It was found that for the calculation of lattice parameters, the PBE and PBE-D3 are in good agreement with experimental values (Table SI) at high and low Li-concentrations respectively. However, PBE functional without any of this correction gives more reasonable data for mechanical properties. To perform electrostatic energy analysis as well as DFT calculations for discharged and charged systems, we modelled the LxCO structure with a space group of R-3m crystal and a unit cell of 2×2×1 ($Li_{12}Co_{12}O_{24}$). A Gamma-centered *k*-point mesh of 4×4×1 and an energy cut-off of 800 eV were applied. Electronic and force convergence criteria of 10^{-5} eV and 10^{-3} eV/Å, respectively, were considered for DFT calculations. For the calculation of elastic constants C_{ij}, we kept fixed the magnetization and atomic coordinates to the optimized ones. C_{ij} matrix was computed using the strain values of 0, ±0.5%, and ±1%. After computing C_{ij}, we obtained the mechanical properties such as Young's, bulk, and shear modulus as well as Poisson's ratio by using the Voigt-Reuss-Hill (VRH) homogenization scheme.[22] To find the most favourable occupation of Li sites by Li ions in L0.50CO, $Li_6Co_{12}O_{24}$, we modelled all possible atomic configurations with various combinations of 6 Li ions in 12 Li sites. We created a total number of 12!/6!6!=924 structures. For charge balancing, we used elementary charges of 1+ for Li, 3.5+ for Co, and 2− for O, respectively. Afterwards, we performed DFT-PBE calculations on 5 distinguishable electrostatically favourable structures and obtained the lowest total energy structure. Total Coulomb

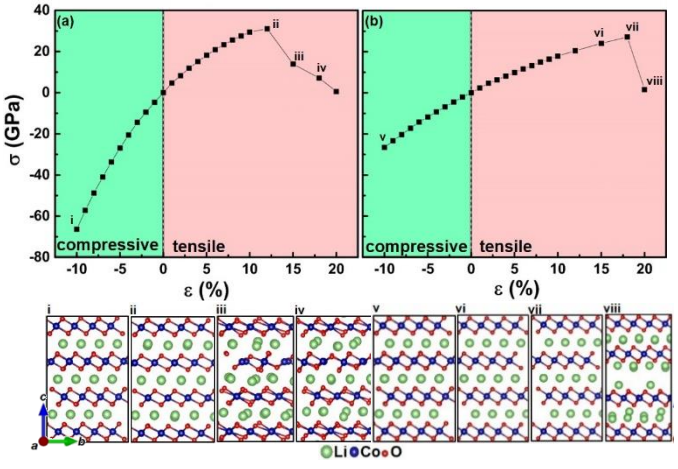

Fig.1. Calculated uniaxial stress (σ) versus strain (ε) in L1.00CO along the (a) *a*- and (b) *c*-direction. Side views of the selected atomic structures are presented at the bottom.

energy calculations were carried out using the so-called *supercell* code.[23] Atomic structures were visualized with the VESTA program.[24] The mechanical response inside the polycrystalline microstructure of LCO was simulated using the grid based solver ElastoDict FeelMath-LD in the software package GeoDict (Math2Market GmbH, Kaiserslautern, Germany).[25-27] To model the LCO microstructure, an experimental microstructure from a FIB-SEM image of a mixed LLZO-LCO cathode from our previous study on solid state batteries[25,28] was used and all LLZO particles were replaced by LCO. The microstructure was segmented into grains using the watershed method (GrainFind module of GeoDict) yielding a median diameter of 2.4 µm. A random set of Euler angles was assigned to each grain resulting in a uniform distribution of orientations. The uncharged (i.e. fully lithiated) particles were assumed to be in the stress-free state. No external forces were applied during the simulation.

Results and Discussions

We first computed the lattice parameters of L_xCO with x=1.0, 0.5, 0.12, and 0.0 (Tab. S1). We found that the parameter a contracts from 2.85 Å to 2.82 Å and c (hereafter it is defined to be 3 intralayer + 3 intralayer separations) expands from 14.01 Å to 14.46 Å for x=1.0 → 0.5. With further delithiation, namely x=0.5 → 0.12 → 0.0, a does not change much, while c decreases significantly as follows a=2.82 Å→2.83 Å→2.82 Å and c=14.46 Å→ 14.35 Å→14.16 Å, respectively. Our results for x=1.0 → 0.5→ 0.12→0.0 are in fair agreement with the reported experimental values of a=2.82 Å → 2.81 Å→ 2.82 Å→ 2.82 Å and c=14.05 Å → 14.37 Å→ 13.54 Å→ 12.87 Å with delithiation reported by Wang *et al*.[31], Zhou *et al*.[6], Chen *et al*.[3] and Amatucci *et al*.[7] Afterwards, the mechanical properties of LxCO with various Li concentrations x and defects were calculated. The computed values of ν for LxCO with various Li concentrations and defects (Table 1) are 0.24–0.25, which agree well with the experimental value of 0.23 and 0.24 reported by Meng *et al*.[29] and Cheng *et al*.[30] We calculated B to be 159.43 GPa for L1.00CO which is slightly higher than the experimental value of 149 GPa reported by Wang *et al*.[31] A previous DFT-PBE study on a defect-free L1.00CO crystal by Wu *et al*.[14] computed Y, B and G to be 252.09 GPa, 166.74 GPa, and 111.38 GPa, respectively, which are even

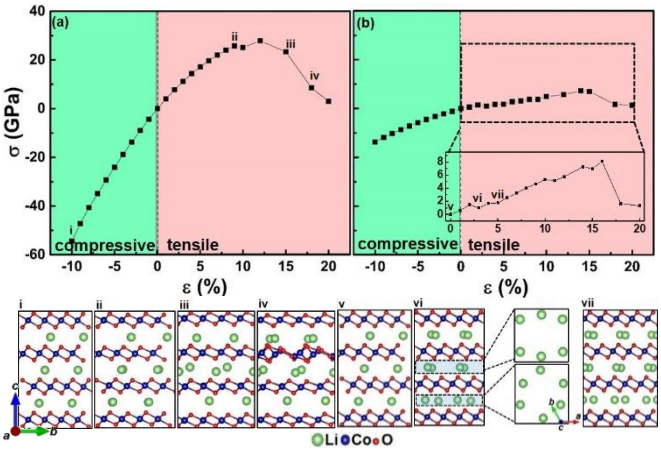

Fig. 2. Calculated uniaxial stress (σ) versus strain (ε) in L0.50CO along the (a) *a*- and (b) *c*-direction. Side views of the selected atomic structures are presented on the bottom.

higher than our calculated values for L1.00CO (Table 1) as well as reported experimental ones.[9,28,32] Yamakawa *et al*.[32] computed the *B* value for LCO to be 146.44 GPa which agrees with the experimental value of 149 GPa[32], but they assumed ν=0.32 in their calculation which is very large compared to the experimental value of 0.23[29] and 0.24.[30] The possible reasons for the difference between our results and those of Yamakawa *et al*.[32] might be the lower cut off energy (500 eV) and less strain points that they used in comparison to our study. The reason of overestimation of *B* in our calculation is most likely due to the fact that a real LCO crystal contains defects at finite temperature. To address this issue, mechanical properties of L1.00CO with Li, Co, or O vacancy (V_{Li}^{x}, V_{Co}^{x}, and V_{O}^{x}) were computed. It is found that the values of mechanical properties decrease in all three defective cases in comparison to the defect-free system (Table 1). The obtained values of *B* become 147.58 GPa and 146.49 GPa for L1.00CO with V_{Co}^{x} and V_{O}^{x}, respectively, which are close to the measured value of 149±2 GPa reported by Wang *et al*.[31] Moreover, with these atomic defects, the magnitudes of *Y* and *G* become smaller and more comparable to the corresponding experimental values (Table 1). In addition, the value of ν remains unchanged and, therefore, it is still comparable to the experimental value.[30] The reason of softening of L1.00CO with the presence of V_{Co}^{x} or V_{O}^{x} vacancies is most likely due to broken Co-O bonds or weakening of electrostatic O-Li-O interaction. Furthermore, we found that the mechanical strength of L*x*CO decreases with delithiation. This is also probably because of the weakening of O-Li-O interaction, *i.e.* interlayer interaction, with delithiation. Our computed delithiation-induced decrease in *B*, *G,* and *Y* is smaller than those computed by Wu *et al*.[14]. Nevertheless, there is no experimental data on delithiated phases to compare with our results.

Afterwards, we computed the stress σ as function of strain ε along *a* (σ_a, ε_a) and *c* (σ_c, ε_c) direction for LxCO. To distinguish the likely effect of delithiation from that of point defects on σ and ε, we first focus on LxCO

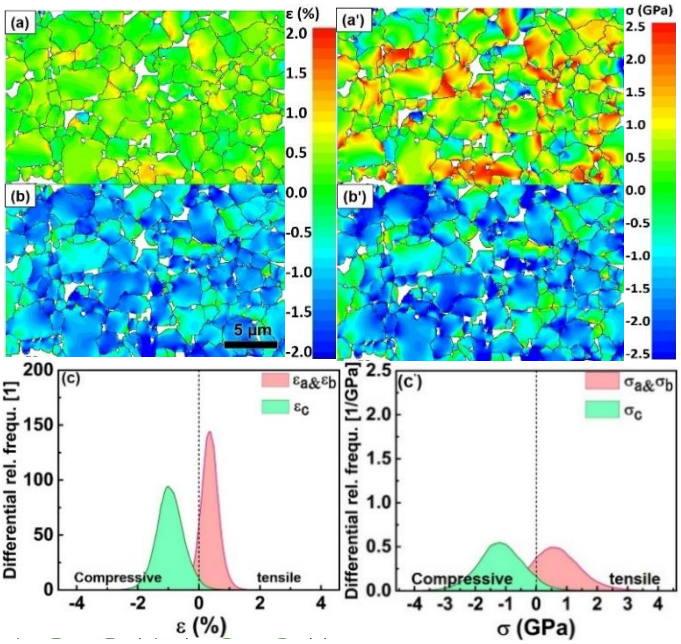

Fig.3. Calculated mechanical stress and strain in an arbitrary microstructure of LxCO induced by the delithiation of its particles from x=1.00 to 0.50: strain distribution along the (a) *a*- and (b) *c*-direction as well as (c) strain histograms along *a*- and *c*-direction; stress distribution along the (a') *a*- and (b') *c*-direction as well as (c') stress histograms along the *a*- and *c*-direction. Fully lithiated particles in the microstructure were assumed to be in the stress-free state. Red and blue colors in (a,b,a',b') represent the tensile and compressive strains and stresses, respectively.

without V_{Co}^{x} and V_{O}^{x}. For L1.00CO (Fig.1), it is found that both σ_a and σ_c drop above large tensile ε_a and ε_c values. The atomic structure of each case undergoes a large displacement under these conditions. Due to the structural phase transition, the σ value drops significantly. Our computed critical strains ($12\% < \varepsilon_a, 18\% < \varepsilon_c$) above which system may experience cracking are, however, clearly much higher than expected values for ceramic materials. Previous theoretical studies by Fang *et al*.[11] and Wu *et al*.[14] have reported even larger critical tensile strains, namely > 30%. Figure 2 shows the computed stress as function of uniaxial strain plot along the *a* and *c* directions for the L0.50CO system. It is found that under compressive ε_a and ε_c as well as tensile ε_a strains the response of Li0.50CO is similar to that of L1.00CO system. However, under tensile ε_c strains, σ_c increases linearly only up to 2% strain. Above this critical strain value, the stress magnitude drops. Previous experimental measurements using advanced scanning transmission electron microscopy (STEM) and high-angle annular dark-field (HAADF) by Yan *et al*.[33] also found intragranular cracking along the (001) orientation in a cycled NCM111 structure. Moreover, we find that the stress drops at 5% and 11% strains as well. Furthermore, we computed the total energy as a function of strain (see Figure S5) indicating phase transitions occurring for $2\% < \varepsilon_c < 3\%$, $4\% < \varepsilon_c < 5\%$, and $10\% < \varepsilon_c < 11\%$. The calculated atomic structures clearly show structural changes at 3%, 5%, and 11% upon which Li ions displace leading to the breaking of their symmetry. Calculated magnetic moment as a function of strain (see Figure S6) shows almost no variation. This indicates that phase transition is driven by the interlayer rather than intralayer O–TM–O interaction. The magnitude of delithiation-induced change in *c* is the determining factor for the critical strain above which restructuring occurs. For example, *c* contracts by 3.4% in L0.12CO with respect to L1.00CO. The computed stress as function of strain for x=0.12 (see Figure S7) shows a phase transition for strain values larger than 6%. The corresponding *c* value of this critical strain is, interestingly, very close the critical *c* value for phase transition in the case of L0.50CO. Displacement of Li-ions in L0.12CO is, however, not similar to that in L0.50CO (Figure S7). This is due to the applied periodic boundary condition for the latter system. We also calculated stress as function of shearing (see Figure S8) in L0.50CO and found that

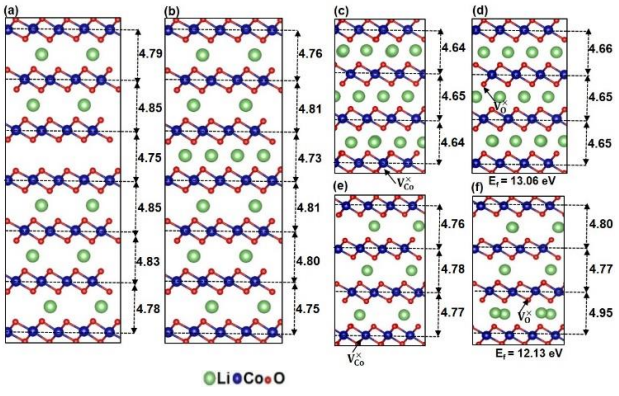

Fig. 4. Calculated Co-Co interlayer separations in L0.50CO with a fully (a) delithiated and (b) lithiated Li layer modelling space charge regions. Calculated Co-Co interlayer separations in L1.00CO and L0.50CO with 4.17 % (c,e) Co and (d,f) O vacancy.

shear strains cannot cause any considerable stress into the system. Hence, no displacements of Li ions are found in this case. However, the calculated stress as function of tensile strain along the *c* direction with an applied fixed shearing strain of 8% shows a similar behavior to the one that was found in Fig. 2.

The Li extraction of x=1.0→0.5 leads to an electrochemically-induced tensile strain of ε_c=2.39% and a compressive strain of ε_a= −0.23% (from the experimental data of Takahashi et al.[34]), but the Li displacement, which can lead to the cracking of a microstructure, occurs only if an additional elastic tensile strain ($\varepsilon_c^{el} > 2\%$) is exerted along *c* in L0.50CO. This means that at least a ≈5% tensile strain along *c* in the L0.50CO system with respect to the equilibrium *c* of L1.00CO system is needed to form cracks in a LCO microstructure. Here, we discuss likely sources of additional 2% tensile strain: I) mechanical strain that arises in each particle of a microstructure from the lattice size change (expansion of *c* and contraction of *a*) of adjacent particles when x=1.00→0.50, II) accumulation or depletion of Li ions in a single Li layer (i.e. sharp space charge), and III) point defects. In the following, we discuss these three possible sources of strains.

I) *Microstructure* We modelled a typical microstructure with randomly oriented particles of arbitrary sizes and computed arising strain/stress due to a delithiation of x=1.00→0.50 within it (see Fig. 3). The anisotropic stiffness matrix that is needed to compute stress/strain distributions in the microstructure was obtained from the DFT-PBE calculation [see Table S2 and the method section for the details of our calculation]. Since our calculated lattice parameters are not much different from the experimental values, we used the corresponding experimental values from ref. 34. Our results show that elastic strains and stresses along *a* are equal to those along *b,* and they are $\varepsilon_a = 0.36\% \pm 0.30$ and $\sigma_a = 0.59 \pm 0.91$ GPa, respectively. However, the corresponding values along the *c*-direction are $\varepsilon_c = -0.94\% \pm 0.56$ and $\sigma_c = -1.2 \pm 0.8$ GPa, respectively. We found that maximum compressive and tensile strains along the *c*-direction are −2.22% and 0.51%, respectively. However, Fig. 2 indicates that tensile lattice strains $\boldsymbol{\varepsilon_c}$ larger than 2% can only lead to cracking. Hence, the delithiation-induced mechanical lattice strains in a microstructure cannot be responsible for an instantaneous failure but it might only cause subcritical crack growth leading to cracking over time.

II) *Sharp space charge SC* To study extreme cases of space charge formation in grain boundaries, we considered a zero (SC0) or full occupation (SC1) of Li sites between two arbitrary adjacent O-Co-O layers. These two cases represent sharp SC areas of fully depleted and accumulated Li layers, respectively (Fig.4(a-b)). The interlayer separation for the fully depleted layer in the SC0 model is 4.75 Å, which is smaller than that for the CoO_2 system with a 1% strain (Figure S9). The interlayer separations for the L0.50CO layers in the SC0 model is 4.78–4.85 Å which are also smaller than those for the L0.50CO system with a

homogenously distributed 0.50Li ions and 1% strain. Since the residual strains are less than 3% (i. e. the starting point of damage), no Li displacement is observed in this SC0 model. The calculated value of interlayer separation for the L1.00CO layer in the SC1 system is 4.73 Å, which is very close to the computed value of 4.72 Å for the L1.00CO system with a 1% strain. The interlayer separations for the L0.50CO layer are comparable to the L0.50CO system with 0%–1% strains. Thus, no displacement of Li is observed for the SC1 model as well. Hence, we find that the space charge cannot be responsible for the microcracking.

III) *Point defect (Co and O Vacancy)* We considered $\mathbf{V_{Co}^{x}}$ and V_O^x (neutral Co and O vacancy) in L1.00CO and L0.50CO, and calculated separations between Co layers $d_{Co\text{-}Co}$ (Fig. 4(c-f)). The calculated values of $d_{Co\text{-}Co}$ in both defective d-L1.00CO systems are similar to those in the defect-free L1.00CO system with a 0% strain. The $d_{Co\text{-}Co}$ distances for d-L0.50CO with V_{Co}^x are also comparable to those in the strain- and defect-free L0.50CO system. However, we find a 3% tensile strain in $d_{Co\text{-}Co}$ in the d-L0.50CO structure in which a 4.17% V_O^x is present. Consequently, the Li ions between O–Co–O interlayers undergo displacements which are very similar to those in the defect-free L0.50CO with a 3% strain. This shows that the displacement of Li ions in the d-L0.50CO structure is only due to the V_O^x-induced expansion of interlayer separation and not a direct V_O^x-Li interaction. The existence of V_O^x leads to a weakening of O-O repulsion and expanding of $d_{Co\text{-}Co}$ leading to the Li displacements. The calculated formation energy of V_O^x is more favourable by 0.93 eV in d-L0.50CO compared to d-L1.00CO. This shows that an increase in the density of O vacancy in the LCO lattice by delithiation (i.e. cycling) can lead to displacements of Li ions and microcracking of LCO cathodes.[35]

Conclusions

In this work, by performing DFT calculation and microstructural mechanical analysis, we investigated the origin of microcracking in LCO. It was found that the defective bulk LCO with O or Co vacancies is softer than its pristine counterpart. Consequently, the mechanical properties of former systems are closer to the experimental measurements. A structural phase transition on the atomic scale (*i.e.* displacements of Li ions) occurs when a tensile uniaxial strain larger than 2% along the *c*-direction (ε_c) is exerted on a defect-free $Li_{0.50}CoO_2$. A similar phase transition is also obtained for $Li_{0.12}CoO_2$ experiencing ε_c > 6% or *c* > 14.80 Å. The critical value of *c* above which Li movement occurs is similar in $Li_{0.12}CoO_2$ and $Li_{0.50}CoO_2$. It is believed that the delithiation-induced mechanical strains in the LCO microstructure is the driving force of cracking. To study this hypothesis, we performed a mechanical GeoDict simulation on an arbitrary cathode microstructure comprising of randomly-distributed L0.50CO particles. It was found that the maximum possible strain (with respect to the strain-free L1.00CO particles) arising from a half delithiation is less than 0.5%. Moreover, our DFT calculation indicates that a heterogeneous

distribution of Li ions between O-Co-O layers, representing a space charge region for example at grain boundaries, cannot lead to a large local tensile strain or restructuring. However, the presence of 4.17% of O vacancy causes a large strain of $\varepsilon_c = 3\%$ leading to the displacements of Li ions. It is known that operating LCO cathodes experience a release of O anions from their lattices. We, therefore, proposed that the delithiation-induced O vacancy formation is the initial stage of microcracking of LCO and most likely the other layered cathode materials.

Author Contributions

N.Y and R.M performed the calculations. N.Y, R.M, O. G., and P. K. analysed the data and wrote the manuscript.

Conflicts of interest

There are no conflicts to declare.

Acknowledgements

The authors gratefully acknowledge financial support from the "Bundesministerium für Bildung und Forschung" (BMBF) as well as the North-German Supercomputing Alliance (HLRN) for providing HPC resources.

Notes and references

1 K. J. Mizushima, P. C. Jones, P. J. Wiseman, J. B. Goodenough, *Materials Research Bulletin.*, 1980, 15, 783-789.

2 B. Huang, Y. I. Jang, Y. M. Chiang, and D. R. Sadoway, *J. Appl. Electrochem*., 1998, 28, 1365–1369.

3 Z. Chen, Z. Lu, and J. R. Dahn, *J. Electrochem. Soc.*, 2002, 149, A1604.

4 H. Wang, Y. Jang, I. Huang, B. Sadoway, *J. Electrochem Soc*., 1999, 146, 473–480.

5 Yoon, W.S., Kim, K.B., Kim, M.G., Lee, M.K., Shin, H.J., Lee, J.M., Lee, J.S. and C.H. Yo, *J. Phys. Chem. B*., 2002, 106,2526–2532.

6 Y.N. Zhou, J. Ma, E. Hu, X. Yu, L. Gu, K. W. Nam, L. Chen, Z. Wang and X. Q. Yang, *Nature communications*, 2014, 5, 1-8.

7 G. G. Amatucci, J. M. Tarascon and L.C. Klein, *J. Electrochem. Soc*., 1996, 143, 1114.

8 T. Ohzuku and A. Ueda, *J. Electrochem. Soc*., 1994, 141, 2972.

9 M. Qu, W.H. Woodford, J.M. Maloney, W.C. Carter, Y.M. Chiang, and V. Vliet, *Adv. Energy Mater*., 2012, 2, 940-944.

10 E.J. Cheng, N. J. Taylor, J. Wolfenstine, and Sakamoto, *Journal of Asian Ceramic Societies*, 2017, 5, 113-117.

11 L. Feng, X. Lu, T. Zhao, and Dillon, *Journal of the American Ceramic Society*,2019, 102, 372-381.

12 Van der Ven, A. Aydinol, M.K. Ceder, G. Kresse, and G. Hafner, *Physical Review B*, 1998, 58, 2975.

13 Y. Qi, Jr. Hector, L.G. James, and C. Kim, *J. Electrochem Soc.*, 2014, 161, F3010- F3018.

14 L. Wu, and Zhang, *Journal of Applied Physics*, 2015, 118, 225101.

15 A. Chakraborty, M. Dixit, D. Aurbach, D.T. Major, *npj Computational Materials*, 2018, *4*, 1-9.

16 P. E. Blöchl, *Phys. Rev. B*., 1994, 50, 17953–17979.

17 G. Kresse and J. Furthmüller, *Phys. Rev. B*., 1996, 54, 11169–11186.

18 J. P. Perdew, K. Burke, and M. Ernzerhof, *Phys. Rev. Lett*., 1996, 77, 3865–3868.

19 S. L. Dudarev, G. A. Botton, S. Y. Savrasov, C. J. Humphreys, and A. P. Sutton. *Phys. Rev. B,* 1998, 57, 1505–1509.

20 L.Y. Kuo, O. Guillon, and P. Kaghazchi, *Journal of Materials Chemistry A*, 2020, 8, 13832-13841.

21 S. Grimme, J. Antony, S. Ehrlich, and H. Krieg, *J. Chem. Phys.,* 2010, 132, 154104.

22 D.H. Chung, and W. R. Buessem, *Journal of Applied Physics,* 1967, 38.6, 2535-2540.

23 K. Okhotnikov, T. Charpentier, and Cadars, *Journal of cheminformatics*, 2016, 8, 1-15.

24 K. Momma, and F. Izumi, *Journal of applied crystallography*, 2011, 44, 1272-1276.

25 R. Mücke, M. Finsterbusch, P. Kaghazchi, D. Fatakowa-Rohlfing, and O. Guillon, *J. Power Sources*., 2021, 489, 229430

26 H. Moulinec and P. Suquet, *Comput. Meth. Appl. Mech. Eng*., 1998, 157, 69-94.

27 M. Schneider, F. Ospald, and M. Kabel, *International Journal for Numerical Methods in Engineering*, 2016, 105, 693-720.

28 R. Elango, A. Demortière, V. De Andrade, M. Morcrette, and V. Seznec, *Advanced Energy Materials*, 2018, *8*, 1703031.

29 M. Qu, W.H. Woodford, J.M. Maloney, W.C. Carter, Y.M. Chiang, and K.J. Van Vliet, *Advanced Energy Materials*, 2012, 2, 940-944.

30 E.J. Cheng, N.J. Taylor, J. Wolfenstine, and Sakamoto, *Journal of Asian Ceramic Societies*, 2017, 5, 113-117.

31 X. Wang, I. Loa, K. Kunc, Syassen, and K. Amboage, *Physical Review B*., 2005, 72, 224102.

32 S. Yamakawa, N. Nagasako, H. Yamasaki, T. Koyama, and R. Asahi, *Solid State Ionics*, 2018, 319, 209-217.

33 P. Yan, J. Zheng, M. Gu, J. Xiao, J.G. Zhang, and C.M. Wang, *Nature communications*, 2017, 8, 1-9.

34 Y. Takahashi, N. Kijima, K. Dokko, M. Nishizawa, I. Uchida, J. Akimoto, *J. Solid State Chem*., 2007, 180, 313–321.

35 C. Sun, X. Liao, F. Xia, Y. Zhao, L. Zhang, S. Mu, S. Shi, Y. Li, H. Peng, G. Van Tendeloo, and K. Zhao, *ACS nano.*, 2020, 5, 6181-6190.